A functional cerebral endothelium is necessary to protect against cognitive decline

Lianne J Trigiani[1] ⓘ**, Miled Bourourou[1], María Lacalle-Aurioles[1],
Clotilde Lecrux[1], Amy Hynes[1], Shoshana Spring[2],
Darren J Fernandes[2]** ⓘ**, John G Sled[2], Frédéric Lesage[3],
Markus Schwaninger[4]** ⓘ **and Edith Hamel[1]**

Abstract

A vascular insult occurring early in disease onset may initiate cognitive decline leading to dementia, while pharmacological and lifestyle interventions can prevent this progression. Mice with a selective, tamoxifen-inducible deletion of NF-κB essential modulator (Nemo) in brain endothelial cells were studied as a model of vascular cognitive impairment. Groups included Nemo[Fl] controls and three Nemo[beKO] groups: One untreated, and two treated with simvastatin or exercise. Social preference and nesting were impaired in Nemo[beKO] mice and were not countered by treatments. Cerebrovascular function was compromised in Nemo[beKO] groups regardless of treatment, with decreased changes in sensory-evoked cerebral blood flow and total hemoglobin levels, and impaired endothelium-dependent vasodilation. Nemo[beKO] mice had increased string vessel pathology, blood-brain barrier disruption, neuroinflammation, and reduced cortical somatostatin-containing interneurons. These alterations were reversed when endothelial function was recovered. Findings strongly suggest that damage to the cerebral endothelium can trigger pathologies associated with dementia and its functional integrity should be an effective target in future therapeutic efforts.

Keywords

Cerebral endothelium, NF-κB essential modulator, physical exercise, simvastatin, vascular cognitive impairment

Received 22 May 2021; Revised 23 July 2021; Accepted 28 July 2021

Introduction

Due to overlap in the cerebrovascular pathology observed in vascular cognitive impairment and dementia (VCID) and Alzheimer's disease (AD),[1,2] we are challenged to decipher the precise role of the vascular contribution to dementia. In post-mortem AD brains, there is increased vessel fibrosis and tortuosity, increased endothelial pinocytosis, disturbance of the blood-brain barrier (BBB), and an increased number of string vessels or capillary remnants that appear as thin strands of connective tissue devoid of endothelial cells.[3,4] Plasma samples from individuals diagnosed with late onset AD reveal elevated biomarkers of endothelial cell (EC) dysfunction such as adhesion molecules and C-reactive protein.[5,6] Of interest, such vascular abnormalities are akin to pathology found in young individuals with *incontinentia pigmenti,* a genetic disorder caused by mutations in NF-κB essential modulator (Nemo) that results in severe neurological symptoms.[3,7] Through activation of NF-kB, Nemo protects

[1]Laboratory of Cerebrovascular Research, Montreal Neurological Institute, McGill University, Montréal, Canada
[2]Mouse Imaging Centre (MICe), Hospital for Sick Children, Toronto, Canada
[3]Biomedical Engineering Institute, École Polytechnique de Montréal, Montréal, Canada
[4]Institute for Experimental and Clinical Pharmacology and Toxicology, University of Lübeck, Lübeck, Germany

Corresponding authors:
Lianne J Trigiani, 3801 University Street, Montreal, QC H3A 2B4, Canada.
Email: Lianne.trigiani@mail.mcgill.ca

Edith Hamel, 3801 University Street, Montreal, QC H3A 2B4, Canada.
Email: Edith.hamel@mcgill.ca

the BBB by stabilizing occludin, and prevents endothelial cell death by reducing oxidative damage.[7] Thus, deletion of Nemo causes the BBB to become more permeable, and increase levels of oxidative stress, both of which are important, early events in the onset of dementia.

Vascular insults occurring early in disease progression have been proposed to initiate cognitive decline seen in neurodegenerative disorders,[8] postulating that such events could disrupt the BBB, which may be an important trigger in dementia pathogenesis.[9,10] This is the basis of the two-hit vascular hypothesis of AD, which stipulates that cerebrovascular damage is sufficient to initiate the cascade of events that lead to neurodegeneration.[11] Correspondingly, a multifactorial, data-driven analysis from longitudinal brain imaging studies revealed that cerebrovascular dysregulation was the first detectable abnormality in the progression of late onset AD.[12] Additionally, a dysfunctional BBB has been identified as an early biomarker of human cognitive dysfunction, independent of the amyloid pathology.[13]

The cerebral endothelium is a key component of the cerebrovascular bed. Vessels are lined with a monolayer of ECs that produce vasoactive substances and ECs are in direct contact with cerebral blood flow (CBF), placing them in a prime position to regulate CBF by reacting to changes in chemical and hemodynamic forces.[14] Brain ECs fulfill roles beyond regulation of cerebral perfusion, namely through neurovascular interactions involving nitric oxide (NO) that are essential for maintaining cognitive health.[15] When cerebral ECs are dysfunctional, the BBB is compromised, allowing neurons and glia to be exposed to toxic substances,[16] and the tight bidirectional communication that exists between neural cells and blood vessels is disrupted.[17,18]

Pharmacological and lifestyle interventions used to control cardiovascular disease have shown promise in preventing or delaying onset of dementia. In a mouse model of VCID, we found that simvastatin (SV, an anti-cholesterol drug) and regular, moderate levels of physical exercise (EX) were effective at preventing cognitive decline.[19,20] Both treatments exert beneficial effects on the brain endothelium: SV by increasing levels of endothelial NO synthase,[21] reducing oxidative stress,[22] and decreasing EC barrier permeability[23]; and while the vascular benefits of EX may extend to the brain,[24] the link is not so well established despite regular EX during midlife being associated with increased levels of endothelial progenitor cells,[25] and improved cerebrovascular function.[26] Growing evidence points to brain ECs as a key mediator of the benefits incurred by EX, including those on cognitive function.[27] However, EX as well as SV have multiple targets, making it difficult to pinpoint the mechanism underlying their protective effects. In the current study we aimed to determine whether cerebral EC function is necessary to reap neuroprotective benefits conferred by these treatments.

Using a tamoxifen-inducible CreER[T2] recombinase mouse model that selectively deletes Nemo in brain ECs under control of mouse Slco1c1 regulatory sequence in mice with a C57BL/6 background,[7] we tested the following hypotheses: (i) Nemo[beKO] (brain endothelial knock-out) mice would show cerebrovascular and behavioural deficits, (ii) SV or EX would be ineffective at protecting against these deficits due to the tamoxifen-induced EC dysfunction, and (iii) deficits would no longer be present after recovery of EC function.

Methods and materials

Animals and treatments

Cohort 1: Four randomly assigned groups of equally distributed male and female mice (3–4 months) were injected with tamoxifen (hereby referred to as cohort 1): 1 group of Nemo[Fl] mice that do not express the Slco1c1-CreER[T2] regulatory sequence ($n = 31$), and 3 groups of Nemo[beKO] mice: one control group ($n = 33$), and 2 groups treated with either SV (~40 mg/kg/day, drinking water, $n = 32$) or EX (3 h free access to a spinning wheel between 7–10 PM, $n = 30$), beginning one month prior to tamoxifen injections, and continued until endpoint (see Supplementary Figure 1). Treatment was interrupted only during tamoxifen administration (5 mg/mL, 50 μL/20 g i.p., twice daily) for 5 days during which we experienced a 10% mortality rate. For EX, each wheel (17.5 cm diameter, Living world, cat #61706) was equipped with a magnetic counter. Based on previously documented appearance and recovery of motor deficits, used as a proxy of endothelial cell function,[7] mice were split into subgroups detailed in Supplementary Figure 1. Six days following the last tamoxifen injection, mice ($n = 11$–15/group) began behavioural testing. Fifteen days after the last injection, mice ($n = 4$–8/group) were used for optical imaging of intrinsic signals. Seventeen days after the last injection vascular reactivity experiments were performed ($n = 4$–5/group). Twenty days after the last injection, BBB integrity was assessed using retroorbital injections of horseradish peroxidase ($n = 5$/group), while other mice were prepared for magnetic resonance imaging ($n = 9$–11/group) or immunohistology ($n = 4$–5/group). *Cohort 2* (hereby referred to as the recovery cohort) included two groups (Nemo[Fl] mice, $n = 17$, and Nemo[beKO] mice, $n = 16$), and was used to investigate whether

allowing EC function to recover was sufficient to regain cognitive function and reverse the observed pathologies. The timing of experiments was as above for cohort 1, with measures repeated after a 3-month recovery period from the initial tamoxifen injection. *Cohort 3* contained two groups (Nemo[Fl] and Nemo[beKO]), and was used to investigate olfactory behaviour, grip strength, and electrophysiology ($n = 13$/group). Mice were housed in a 12-hour light-dark cycle with food and water *ad libitum*. Experiments were approved by the Animal Ethics Committee of the Montreal Neurological Institute and complied with the Canadian Council on Animal Care, and ARRIVE 2.0 guidelines[28] complied with as closely as possible.

Behavioural tests

Morris water maze (MWM). Spatial cognitive function was evaluated in the Morris water maze,[29] as previously described.[30] A pool (1.4 m diameter) was filled with water (18 ± 1°C), made opaque with inert white paint. Three visible platform training days were performed: On each day, the mice were given three trials of 60 s separated by approximately 45 min to find the platform (15 cm diameter). Before the 5-day learning phase of the task, visual cues and location of the platform were changed. Mice were given three trials of 90 s to find the hidden platform (submerged 1 cm below water). On the final day, a probe trial was conducted to assess spatial memory. The platform was removed, and mice were given 60 s of free swimming. The duration and total distance in the quadrant that contained the platform was recorded, as well as the number of times the mice would have landed on the platform if present. Data were recorded using the 2020 Plus tracking system and Water 2020 software (Ganz FC62D video camera; HVS Image, Buckingham, UK).

3-Chamber sociability test. An early symptom of dementia includes social withdrawal, which was tested using a sociability test whereby mice were habituated to a plexiglass testing arena split into 3 chambers for 10 min before undergoing 20 min of testing the following day. In the first 10 min, the mouse was given the option to interact with either an empty plexiglass cylinder in one chamber, or with a cylinder containing a stranger mouse in another chamber. Being social animals, mice tend to explore the chamber containing the stranger mouse. After 10 min, the mouse was removed from the testing arena while a second stranger mouse was placed in the previously empty cylinder. The mouse was then placed back into the testing area for another 10 min to assess social preference, where the expectation is that healthy control mice will spend more time interacting with the new stranger mouse.

Nesting behaviour. Just before their dark cycle, mice were placed into individual cages with 3.0 g of packed nesting material (no hut or additional enrichment). The following morning mice were carefully removed and placed in their original cages to assess the quality of the nest on a qualitative scale from 1 to 5 based on criteria provided by Deacon,[31] with a score of 1 indicating >90% of nesting material was untouched, and a score of 5 being the most complex nest.

Cerebrovascular reactivity

Endothelial function of isolated middle or posterior cerebral arteries *(n = 4–5/group)* was measured with online video microscopy (Living Systems Instrumental, Burlington, VT), as before.[32] Vessel segments were gradually pressurized over 10 min to reach 60 mmHg and allowed to develop resting tone. Responses to endothelium-dependent dilators acetylcholine (ACh, 10^{-10}–10^{-4} M; Sigma Aldrich, Oakville, ON) and TRPV4 channel opener GSK1016790A (GSK, 10^{-10}–10^{-5} M; Sigma Aldrich, Oakville, ON), and smooth muscle relaxant NO donor sodium nitroprusside (SNP, 10^{-10}–10^{-5} M; Sigma Aldrich, Oakville, ON) were tested on pre-constricted vessels (phenylephrine 2×10^{-7} M; Sigma Aldrich, Oakville, ON). Responses were expressed as percentage change in diameter from pre-constricted vessels and plotted as a function of vasodilator concentration. Concentration-dependent and maximal (EA_{max}) responses were used to compare vasodilator efficacy.

Imaging of optical intrinsic signals (OIS)

Two weeks prior to being injected with tamoxifen, mice were implanted with cranial windows (4 mm glass) glued on a thinned bone preparation over the left barrel cortex. Two weeks after the first tamoxifen injection, mice were anesthetized (ketamine 85 mg/kg/xylazine 3 mg/kg, i.m.) and fixed through ear bars on a physiological platform (Harvard Apparatus #75-1500, Saint-Laurent, Canada) with online recording of temperature, heart and respiratory rates. The platform was moved to the imaging system (OIS200 from LabeoTech, Montréal, Canada); and the cranial window was placed parallel to the camera (Figure 2 (e)). Whisker-evoked changes in total, oxy- and deoxyhemoglobin (HbT, HbO and HbR, respectively) were measured with light-emitting diodes (LEDs, 525 m 590 and 625 nm). Whisker-evoked changes in CBF were measured with laser speckle contrast imaging using a 780 nm laser diode. Images were acquired at a frame rate of 30 Hz in total (7.5 Hz for each wavelength), with a 14 ms exposure time. Each recording consisted of 7 blocks of right whisker stimulation

(8 Hz, 20 s followed by 40 s of rest using a piezo actuator, Q220-A4-303YB, MA, USA). A 3 s jitter was included to avoid habituation of stimulation timing. Data were filtered at 0.3 Hz to suppress high frequency noise and analyzed using MATLAB to obtain changes in cerebral blood volume and CBF from baseline, as described in Dubeau et al. 2011.[33] Reflectance signals were converted to changes in absorption $\Delta A = \log(R/R_0)$, and a pseudo-inverse and the modified Beer–Lambert law were used to extract relative changes in HbR and HbO. CBF was computed by quantifying the spatial contrast during laser illumination, defined as the ratio of the standard deviation to the mean intensity in a given spatial area. For each animal, a region of interest around the maximum response was manually delineated and contributions from medium and large arteries and veins were removed. The signal was averaged over all pixels in the region of interest to recover an impulse response function for each component: HbO, HbR and CBF. These experiments were repeated 3 months later, after the recovery period in cohort 2.

Electrophysiology recording (ECog)

In cohort 3, fifteen days after the last tamoxifen injection, mice were anesthetized with Ketamine/Xylazine (85 mg/kg, i.m.), and placed on a physiological platform as above. Barrel cortex was exposed by drilling the overlaying cranial bone. A 32-channel micro-ECoG (Electrocorticogram) electrode array (Neuronexus, E32-600-10-100-H32, MI, USA) was placed on the dura, then covered with warm agarose gel (1%) and glass coverslip. A screw on the cerebellum was used as a reference. Whiskers were attached to a piezo actuator and stimulated at 1, 2 and 4 Hz for 5 sec and 8 Hz for 20 sec. Data were acquired at a 30 kHz sampling rate by an OpenEphys system (open-ephys.org) and analyzed using a custom-made MATLAB script. P1-N1 amplitude of the evoked responses was computed as the maximum and the minimum values over the initial 62.5 ms of each trigger. First P1-N1 amplitude was based on the first peak of each stimulation train, while the mean P1-N1 was the average over all the pulses of each stimulation train. Signal was decomposed in frequency band powers (Theta: 4–8 Hz, Alpha: 8–12 Hz, Beta: 15–30 Hz, Gamma: 40–55 Hz and High gamma: 80–150 Hz), and evoked changes in power were normalized from baseline epoch.

Magnetic resonance imaging (MRI)

A multi-channel 7.0 Tesla MRI scanner (Varian Inc., Palo Alto, CA) was used to image brains ($n = 8$–10/group) within their skulls following perfusion with 30 mL of 1 M phosphate buffered saline (PBS) containing 30 μL heparin and 2 mM gadolinium followed by 30 mL of 4% paraformaldehyde (PFA) containing 2 mM gadolinium (rate of 1 mL/min). Brains were stored (4°C) in 1 M PBS containing 2 mM gadolinium and 0.02% sodium azide for 3 months. Sixteen custom-built solenoid coils were used to image the brains in parallel.[34]

Anatomical scan. To detect volumetric changes, we used the following parameters for the MRI scan: T2-weighted, 3-D fast spin-echo sequence, with a cylindrical acquisition of k-space, a TR of 350 ms, and TEs of 12 ms per echo for 6 echoes, field-of-view (FOV) of $20 \times 20 \times 25$ mm^3 and matrix size of $504 \times 504 \times 630$. Parameters produced images with 0.040 mm isotropic voxels. The total imaging time was 14 hours.

Diffusion tensor imaging. Diffusion Tensor Imaging (DTI) was performed using a 3D diffusion weighted fast spin-echo sequence (FSE), with an echo train length of 6. Parameters for the DTI sequence were: TR = 270 ms, first TE = 32 ms, and a TE of 10 ms for the remaining 5 echoes, 1 average. FOV of $14 \times 14 \times 25$ mm^3 and a matrix size of $180 \times 180 \times 324$ yielded images with 78 μm isotropic voxels. Five $b = 0$ s/mm^2 images were acquired and 30 high b-value ($b = 2147$ s/mm^2) in 30 different directions were acquired, using the Jones30 scheme.[35] Total imaging time was ∼12 hours. After acquisition, images were analyzed using the FSL software package (FMRIB, Oxford UK), which was used to create fractional anisotropy (FA), mean diffusivity (MD), and axial diffusivity (AD) maps for each brain.

MRI registration and analysis. To visualize and compare changes in the mouse brains, images ($b = 0$ s/mm^2 images for DTI) were linearly (6-followed by 12-parameter) and non-linearly registered together. Registration and analysis workflow has been previously described.[36] Registrations were performed with a combination of mni_autoreg[37] and advanced normalization tools.[38] All scans were then resampled with the appropriate transform and averaged to create a population atlas representing the average anatomy of the study sample.

Prior to statistical analysis, logarithms of the Jacobian determinants were taken to eliminate skewness. For diffusion measurements, the registration allowed for analysis of the intensity differences of all measures (FA, MD, and AD) between genotypes. Significant volume changes and intensity differences could then be calculated by warping a pre-existing classified MRI atlas onto the population atlas, allowing for the volume or mean diffusion measure of different segmented structures.[39,40] To assess significance, linear

models were fitted to the mean diffusion measures for each structure, with group as the independent variable. The False Discovery Rate was used to control for multiple comparisons across structures.[41] One-way ANOVAs were conducted for structures of interest and results are shown using these statistics, which revealed the same results as the linear model with false discovery rate, with the exception of the right olfactory tubercle.

Immunohistochemistry

The remaining mice from each group ($n = 4–5$/group, 2–3 sections/mouse) were anesthetized (65 mg/kg of sodium pentobarbital, i.p.) and perfused using 4% PFA in phosphate buffer (PB; 0.1 M, pH 7.4). Brains were post-fixed in 4% PFA-PB overnight, cryoprotected (30% sucrose, 48 h), frozen in isopentane and stored at $-80°C$. Coronal sections (25 μm) were immunostained (overnight) as floating sections. Antibody sources and concentrations are listed in supplementary table 1. We stained for reactive astrocytes (anti-GFAP), reactive microglia (anti-Iba-1), microglia responding to injury (anti-galectin-3), resident microglial cells (anti-TMEM-119) and infiltrating peripheral immune cells (anti-CD45), neuronal markers included choline acetyltransferase (anti-ChAT), somatostatin (anti-SOM), parvalbumin (anti-PV), and pro-cholecystokinin (anti-pro-CCK)[42] and vessel basement membrane using anti-collagen IV following heat-mediated antigen retrieval. After rinsing, sections were incubated (30 min) with species-specific Cy2-tagged secondary antibodies for immunofluorescence detection (cy2 1:400). For ChAT immunolabeling, biotinylated anti-goat (1:200, Vector Laboratories) was used as a secondary antibody followed by incubation in the avidin-biotin complex (75 min, Vector Laboratories), and immunodetection with 3′3-diamino-benzidine (DAB) staining kit (Vector Laboratories). Sections were then mounted on gelatin-coated slides, coverslipped with mowiol (fluorescence) or dehydrated and coverslipped with Permount (DAB). Anatomical markers were quantified in the cerebral cortex and the corpus callosum, an easily identifiable WM tract that myelinates early during development, making it less vulnerable to damage than late-myelinating structures.[43] The percentage area occupied by an antibody (GFAP, Iba-1, Galectin-3, pro-CCK) and cell counts (SOM, PV, ChAT) were measured using ImageJ software. The number of string vessels were counted directly under the microscope.

Hemosiderin staining. Coronal sections (25 μm) were acquired from brains used for MRI imaging. The iron staining solution was prepared with equal volumes of potassium ferrocyanide and hydrochloric acid solutions (ab150674 kit, Abcam) and slides immersed for a 3 min incubation, rinsed in distilled water, then stained in the nuclear fast red solution (5 min), rinsed (4x) in distilled water, dehydrated in alcohol, and cover-slipped using Permount.

Horseradish peroxidase injections and staining. Mice were anesthetized with isoflurane to inject horseradish peroxidase (HRP) type II (Millipore Sigma, catalog #P8250; 0.5 mg/g) dissolved in 0.4 mL of 0.1 M PBS, and injected retro-orbitally (0.2 mL/sinus). HRP circulated for 30 min before the mouse was then euthanized. The brain was dissected and placed in 4% PFA/0.1M PB at 4°C overnight. The following day, brains were placed in PBS prior to vibratome sectioning (Harvard Apparatus, Vibratome 1000 Classic, Saint-Laurent, QC, Canada). Sections (50 μm) were incubated in DAB (35 min), mounted on gelatin-coated slides, dehydrated and cover-slipped with Permount.

Statistical analysis

All *in vivo* experiments were performed blind. One-way ANOVAs followed by a Newman-Keuls *post-hoc* multiple comparison test and independent samples *t*-tests were conducted using GraphPad Prism 7. Due to swimming speed being a confounding variable for the MWM analysis, ANCOVAs were performed using swimming speed as the covariate. A *p* value ≤ 0.05 was considered statistically significant.

Results

Data and MATLAB scripts are available from the corresponding authors upon reasonable request.

Cerebral EC dysfunction induces motor and cognitive deficits that are not overcome by SV and only mildly protected by EX

Nesting is a natural, highly motivated behaviour in both male and female mice, and thus changes in nesting indicate a change in the animal's overall welfare,[44] similar to an assessment of quality of life in human patients. Nemo[beKO] mice made less complex nests following tamoxifen ($F(3, 50) = 8.01$, $p < 0.001$), and neither SV or EX ($p < 0.01$) preserved nesting behaviour seen in Nemo[Fl] mice (Figure 1(a)). When Nemo[beKO] mice were given 3 months to recover from the effects of tamoxifen, the quality of nests was indistinguishable from that of Nemo[Fl] mice ($t(20) = 0.23$, $p > 0.05$, Figure 1(c)). Nemo[beKO] mice were impaired when assessed for social preference (Figure 1(b), $t(26) = 0.27$, $p > 0.05$), indicating either social impairment
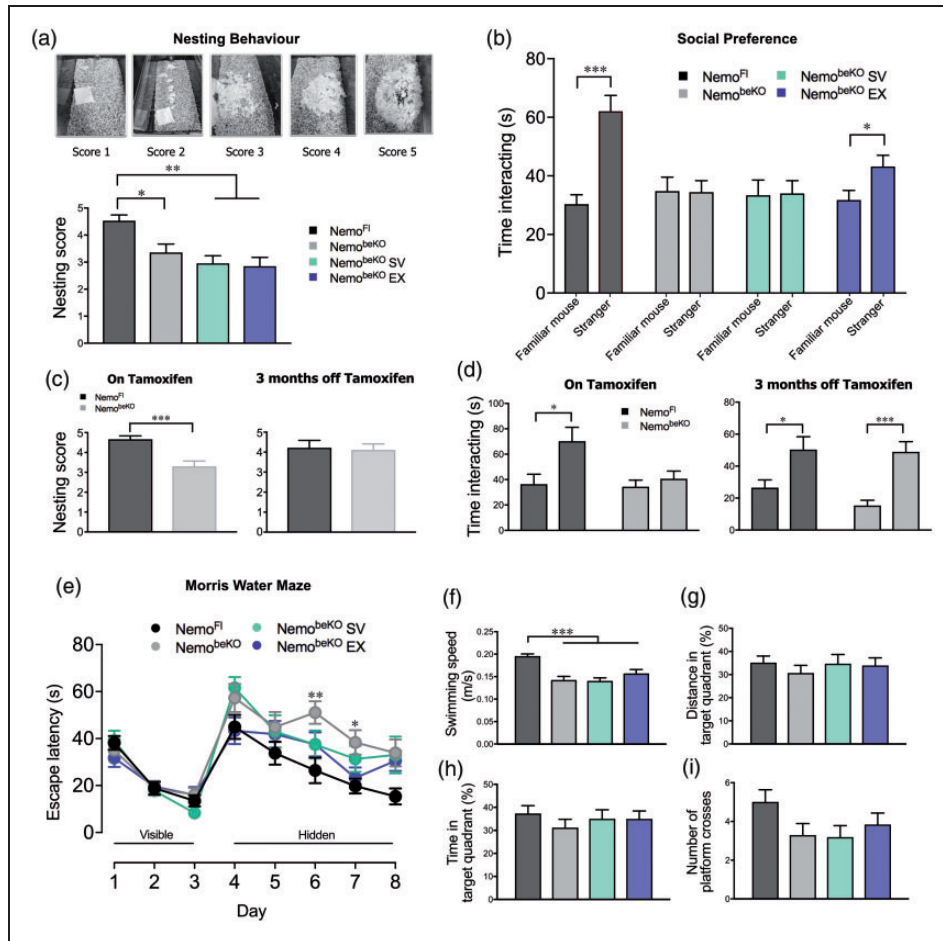
Figure 1. Nemo[beKO] groups had significantly lower nesting scores (a) and impaired social preference assessed by the 3-chamber sociability test (b). This same observation was made in Nemo[beKO] mice injected with tamoxifen in the recovery cohort; however, after being given 3 months to recover, Nemo[beKO] mice performed just as well as control Nemo[Fl] mice (c and d). Cognitive deficits observed on days 6 and 7 of the spatial learning phase of the Morris water maze (e) were attributed to decreased swimming speed that was recorded on each testing day for all groups. No deficits were detected during the spatial memory probe (f–i), trend in reduced platform crossings for Nemo[beKO] groups regardless of treatment being attributable to impaired motor function evidenced by slower swimming speeds (f). Paired sample t-tests were performed for each group to compare time spent with individual mice for the sociability test. $N = 12–15$ mice/group, one-way ANOVA with post-hoc Newman-Keuls multiple comparison tests were performed for nesting behaviour and ANCOVA for Morris water maze performance controlling for swimming speed as the covariate. $*p < 0.05$, $**p < 0.01$, $***p < 0.001$.

or inability to distinguish between the mice, as previously reported.[7] This impairment was also observed in mice treated with SV ($t(20) = 0.05$, $p > 0.05$), but not in the EX group ($t(24) = 2.46$, $p < 0.05$), indicating a mild protective effect of EX. In the recovery cohort, the impairment observed in Nemo[beKO] mice (Figure 1(d), $t(24) = 0.82$, $p > 0.05$), was no longer present when taken off tamoxifen ($t(24) = 4.81$, $p < 0.001$). Nemo[beKO] mice had poorer habituation and dishabituation scores (Supplementary Figure 2 (a) and (b), respectively) in the olfactory discrimination test. This indicated olfactory alterations or poor olfactory memory, as the Nemo[beKO] mice needed more time to recognize the same odour and had more difficulty distinguishing between odours,

significantly so between the two social odours ($t(21) = 3.04$, $p < 0.01$). Regardless of treatment, Nemo[beKO] mice showed no deficits in spatial learning or memory in the Morris water maze compared to Nemo[Fl] mice (Figure 1(e) to (i)). Differences in the latency to reach the hidden platform (Figure 1(e)) were likely due to slower swimming speeds noted during the spatial learning phase (data not shown), and no significant differences in spatial memory were observed on a probe trial (Figure 1(g) to (i)). Motor deficits were confirmed in the wire hang test (Supplementary Figure 2(c)), whereby Nemo[beKO] mice had poorer grip strength typified by shorter latency to fall from a wire cage compared to Nemo[Fl] mice.

Cerebral EC dysfunction results in functional and anatomical cerebrovascular alterations that are not overcome by EX or SV

Disrupting Nemo in brain ECs had deleterious effects on endothelium-dependent dilation in isolated cerebral arteries, shown here by ACh and TRPV4 channel opener GSK1016790A dilations being reversed to constrictions (Figure 2(a) and (b)), while dilation to smooth-muscle relaxant NO donor SNP was unaltered (Figure 2(c)). More interesting is the lack of effect SV or EX had on vasodilatory function, whereby vessels treated with SV responded identically to those of untreated Nemo[beKO] mice. Nemo[beKO] mice treated
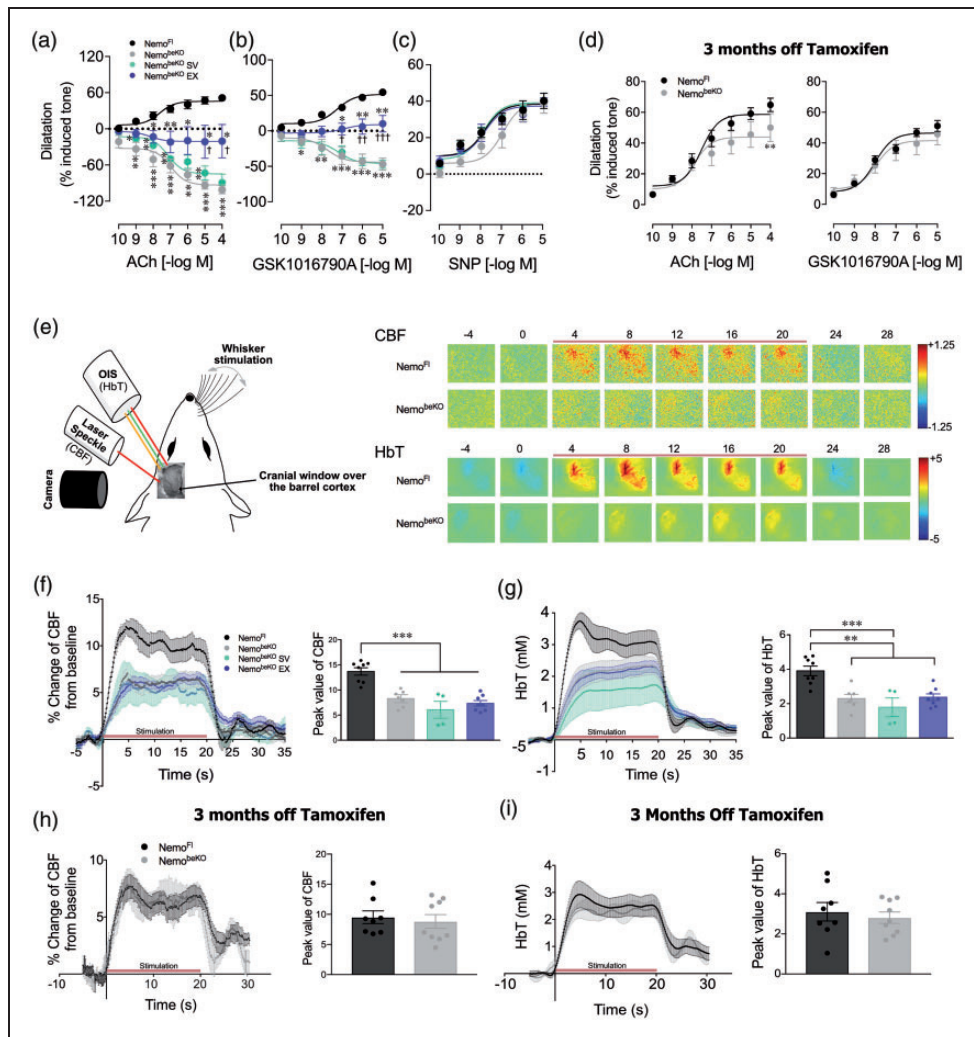
Figure 2. Cerebrovascular reactivity tested in isolated cerebral arteries showed that Nemo[beKO] mice had impaired responses to endothelium-dependent dilators acetylcholine (ACh) and TRPV4 channel opener (GSK1016790A), now being reversed to constrictions (a and b). In contrast, the dilatory responses to the smooth muscle relaxant NO donor sodium nitroprusside (SNP) were unaltered (c). Similar findings were seen in mice treated with simvastatin (SV) that significantly differed from both Nemo[Fl] and Nemo[beKO] mice that exercised (EX) at several concentrations of ACh and GSK1016790A. Nemo[beKO] EX mice showed significantly improved responses but these still remained different from controls (A and B). In the recovery cohort, cerebral vessels dilated well and only differed from control Nemo[Fl] mice at the highest ACh concentration (d). $N = 4$-5 mice/group. One-way ANOVA with post-hoc Newman-Keuls multiple comparison tests were performed *,†$p < 0.05$, **,††$p < 0.01$, ***, †††$p < 0.001$ compared Nemo[Fl] control mice or to other Nemo[beKO] groups. Schematic representation of the setup used in mice with cranial window over the barrel cortex to measure hemodynamic responses to whisker stimulation using laser speckle contrast imaging (LSCI) and optical imaging of intrinsic signals (OIS) (e, left). Representative time course of changes in cerebral blood flow (CBF) and total hemoglobin (HbT) levels evoked by 20 s whisker stimulation (indicated by red bar) (E, right). Regardless of treatments, Nemo[beKO] mice had significantly lower CBF (f) and HbT (g) whisker-evoked responses. In the recovery cohort, no differences between groups were observed in CBF (h) and HbT (I). $N = 4$–8 mice/group. One-way ANOVA with post-hoc Newman-Keuls multiple comparison tests were performed **$p < 0.01$, ***$p < 0.001$.

with EX continued to have contractile or impaired dilatory responses significantly different from Nemo^{Fl} control mice whose vessels dilated. However, the persisting impairments in the EX group were significantly reduced compared to both SV and untreated Nemo^{beKO} mice at higher ACh and GSK1016790A concentrations ($p < 0.05$ to 0.001), pointing to some benefits of EX. In the recovery cohort, Nemo^{beKO} vessels dilated in response to ACh and GSK1016790A to the same extent as vessels from control Nemo^{Fl} mice except at the highest ACh concentration ($p < 0.01$) (Figure 2(d)). In response to whisker stimulation, regardless of treatment, Nemo^{beKO} mice had lower CBF peak values ($p < 0.001$, Figure 2(f)) and lower total hemoglobin (HbT) levels ($p < 0.01$ or 0.001, Figure 2(g)) compared to Nemo^{Fl} mice; the latter driven by changes in oxygenated hemoglobin levels rather than deoxygenated hemoglobin (data not shown). Whisker-evoked CBF and HbT responses were both indistinguishable from Nemo^{Fl} mice in the recovery cohort (Figure 2(h) and (i)).

Additional evidence of cerebrovascular pathology in Nemo^{beKO} mice included enhanced ($p < 0.001$) string vessel pathology in the cortex and corpus callosum (Figure 3(a)); SV ($p < 0.01$) and EX ($p < 0.05$) slightly improved this pathology only in WM. In the recovery cohort, string vessels remained significantly more numerous than in Nemo^{Fl} mice ($p < 0.001$ in the cortex, $p < 0.05$ in the corpus callosum), but they were 2 to 3-fold fewer than in Nemo^{beKO} mice on tamoxifen. In order to assess disruption of the BBB, a 44 kDa protein (HRP) was injected retro-orbitally
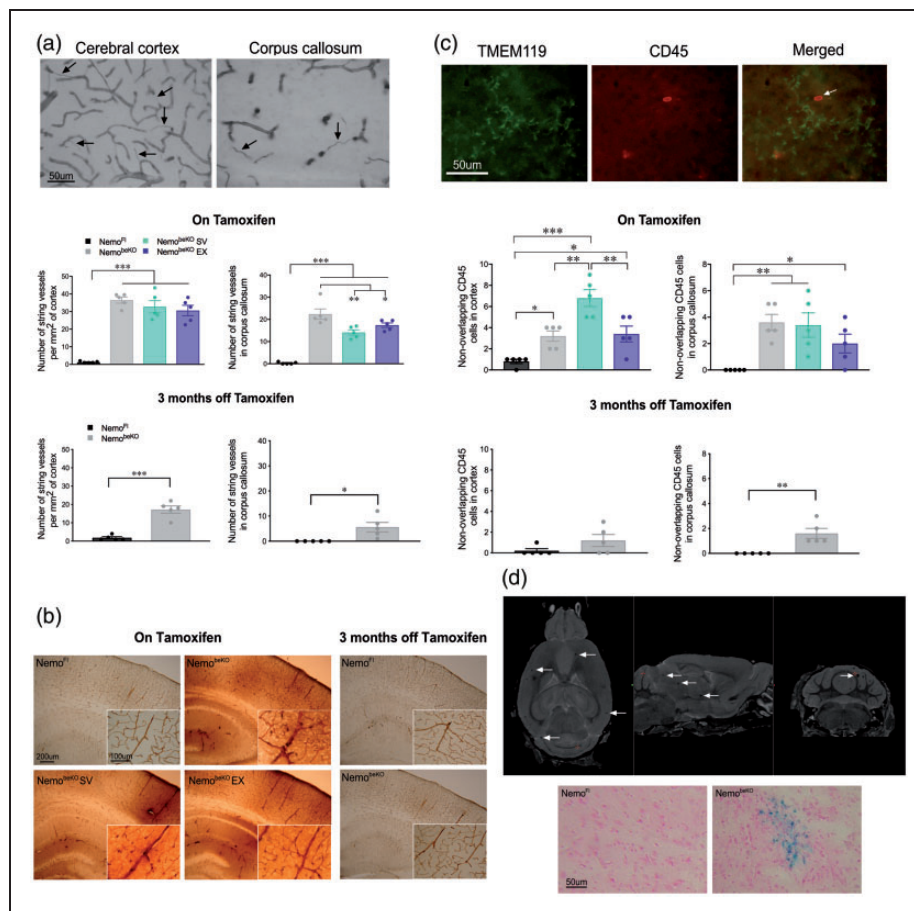

Figure 3. Staining with collagen IV revealed increased number of string vessels in the cerebral cortex and corpus callosum of Nemo^{beKO} mice that remained elevated although to a much lesser extent in the recovery cohort (a). Retro-orbital injections of horseradish peroxidase and resultant visualization with DAB staining showed evidence of BBB leakage in Nemo^{beKO} mice that was no longer present after 3 months off tamoxifen (b). Infiltration of circulating leukocytes (CD45, red), not colocalized with microglial marker TMEM119 (green), was increased in all Nemo^{beKO} groups, particularly in the cortex of Nemo^{beKO} simvastatin (SV) group; this infiltration was decreased in the recovery cohort (c). Microbleeds were identified by magnetic resonance imaging as small black dots (white arrows) in Nemo^{beKO} mice regardless of treatment, while none were visualized in Nemo^{Fl} mice, as confirmed *ex vivo* using an iron stain (d). $N = 4$–5 mice/group. One-way ANOVA with post-hoc Newman-Keuls multiple comparison tests were performed **$p < 0.01$, ***$p < .001$.

and visualized with DAB (Figure 3(b)). HRP was contained within the blood vessels of all groups, however, Nemo^{beKO} mice also displayed strong HRP staining in brain parenchyma regardless of SV or EX treatment. This parenchymal labeling was not observed in the recovery cohort after 3 months without tamoxifen (Figure 3(d)). As further indication of a leaky BBB, double-labeled TMEM119 and CD45 immune cells were quantified. The number of CD45-positive cells but TMEM119-negative, considered as peripheral immune cells entering the brain, was significantly increased in the cortex ($p < 0.05$) and corpus callosum ($p < 0.01$) of Nemo^{beKO} mice compared to Nemo^{Fl}, and particularly so in the cortex of Nemo^{beKO} mice treated with SV ($p < 0.001$) (Figure 3(c)). This increase in CD45 infiltrating cells was no longer significant in the cortex of the recovery cohort, but it persisted in the corpus callosum ($p < 0.01$).

Cerebral EC dysfunction results in microbleeds and poorer WM integrity that are exacerbated by SV and not overcome by EX

In anatomical brain images obtained by MRI, evidence of microbleeds appeared as small black dots that were confirmed with hemosiderin stain for iron deposits in tissue sections (Figure 3(d)). These dots were not observed in Nemo^{Fl} mice but were present in 9/11 Nemo^{beKO} mice, 8/9 Nemo^{beKO} EX mice, and 10/10 Nemo^{beKO} SV mice. We also noted that all Nemo^{beKO} groups had larger brain volumes (data not shown) compared to Nemo^{Fl} brains, likely due to edema. The DTI analysis revealed that Nemo^{beKO} mice tended to have higher axial diffusivity in motor-related areas (pyramidal tracts and inferior olivary complex). Whereas EX mice were indiscernible from Nemo^{Fl} mice, mice treated with SV fared worse ($p < 0.01$ for axial diffusivity), likely due to the lowering of endogenous cholesterol synthesis in the brain (Figure 4(b), (d), and (e)). A higher axial diffusivity was observed in the olfactory tubercle of Nemo^{beKO} SV mice, providing some insight into the poorer performance of Nemo^{beKO} mice on the olfactory discrimination test.

EX and SV did not recover neuroinflammation induced by cerebral EC dysfunction

When quantifying the level of reactive astrocytes in the cortex, we found that Nemo^{beKO} mice, regardless of treatment, showed significantly more GFAP labeling ($p < 0.001$) compared to Nemo^{Fl} mice, which was indistinguishable from controls in the recovery cohort (Figure 5(a) and (b)). Nemo^{beKO} mice with and without
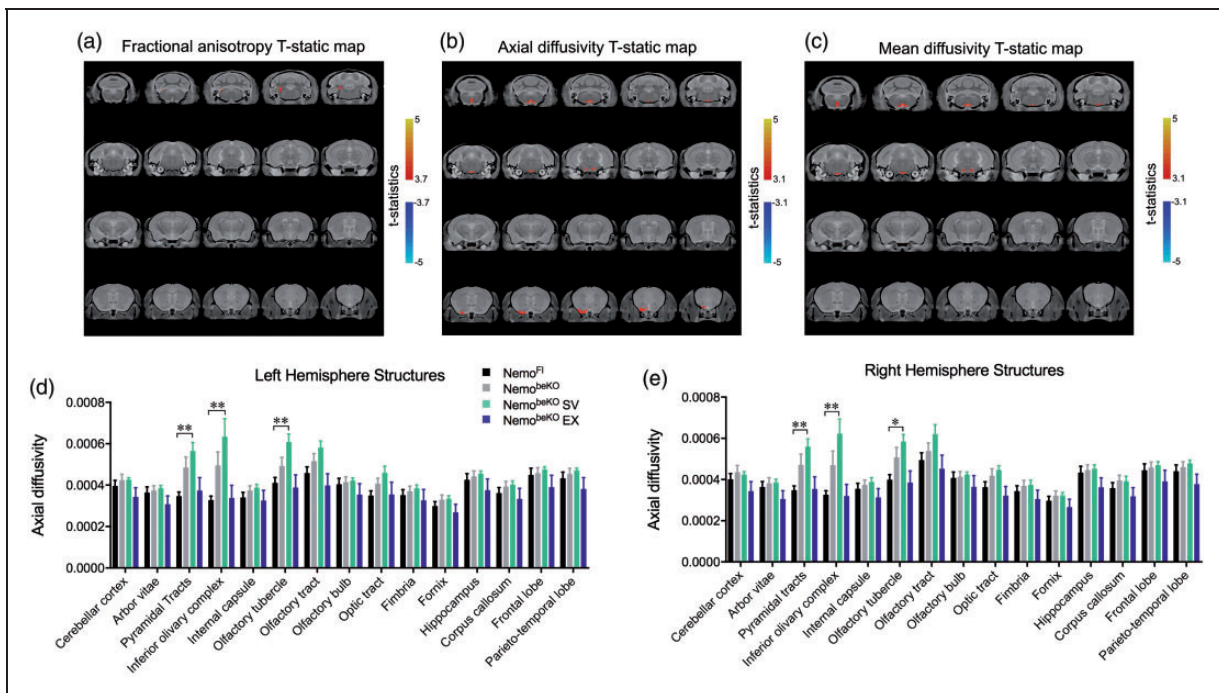

Figure 4. Diffusion tensor imaging analysis from magnetic resonance imagining images including fractional anisotropy (A), axial diffusivity (B), and mean diffusivity (C) with statistical threshold shown whereby Nemo^{beKO} mice treated with simvastatin (SV) are significantly different in both left (D) and right hemisphere (E) structures including the pyramidal tract, olfactory tubercle, and inferior olivary complex. One-way ANOVA with post-hoc Newman-Keuls multiple comparison tests were performed for each structure of interest for axial diffusivity. $N = 8–10$ mice/group, $*p < 0.05$ and $**p < 0.01$.
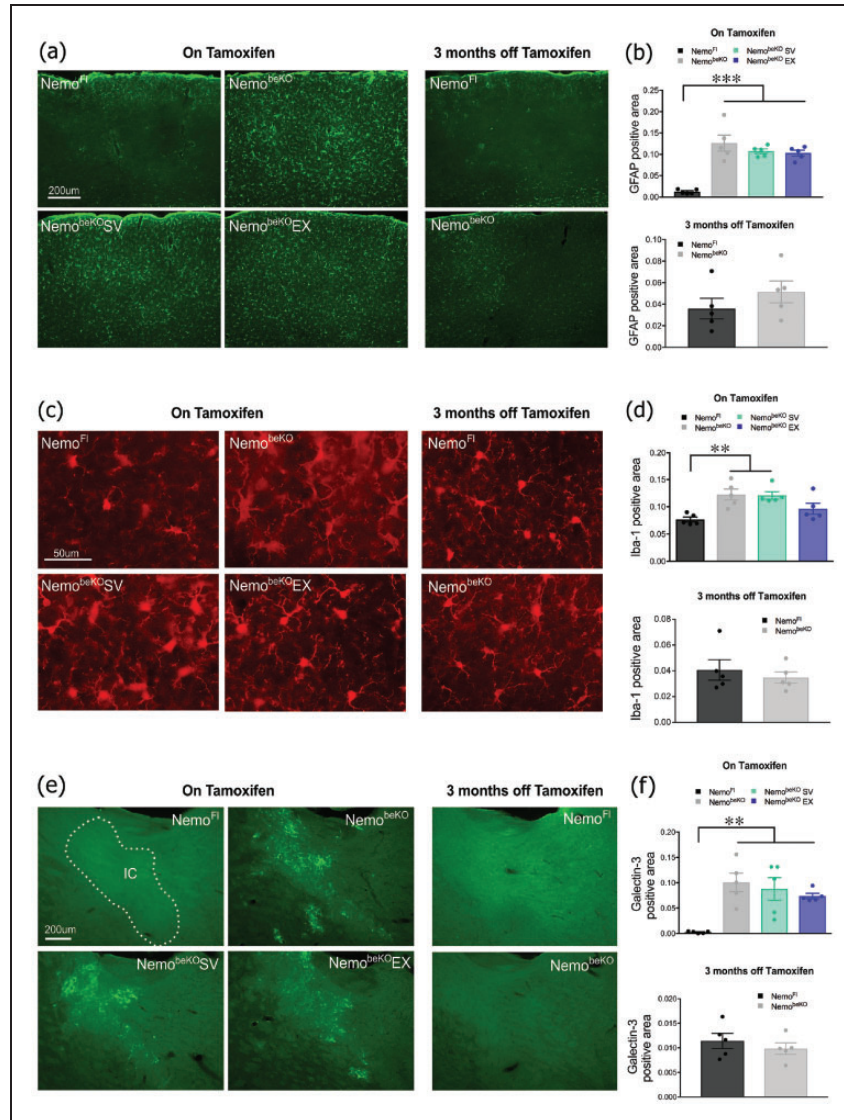
Figure 5. Astrogliosis detected with GFAP immunofluorescence was significantly increased in the cortex of all Nemo[beKO] groups regardless of treatment but returned to normal in the recovery cohort (A and B). Microglial activation in the cortex was also significantly raised in the Nemo[beKO] groups as quantified by Iba-1 positive area, with the exception of mice that exercised (EX) and returned to normal in the recovery cohort (C and D). Inflammation in the internal capsule (IC) was increased in all Nemo[beKO] groups identified by galectin-3-positive microglial cells, a response completely normalized in the recovery cohort (E and F). $N = 4$–5 mice/group. One-way ANOVA with post-hoc Newman-Keuls multiple comparison tests were performed $**p < 0.01$, $***p < .001$.

SV treatment also had more extensive Iba-1 labeling in cortical microglia ($p < 0.01$); however, Nemo[beKO] mice treated with EX were not significantly different from control Nemo[Fl] mice, as was also the case in the recovery cohort (Figure 5(c) and (d)). Microglia in WM tracts (shown here in the internal capsule) labeled with galectin-3 were also strikingly increased ($p < 0.01$) in Nemo[beKO] mice, a response not affected by SV or EX and fully normalized in the recovery cohort with restored EC function (Figure 5 (e) and (f)).

Cerebral EC dysfunction alters neuronal activity and populations: effects of SV and EX

Astrocytic activation and BBB dysfunction have been posited to be the cause of epileptic seizure activity found in Nemo[beKO] mice.[7] Here, we further explored this cortical hyperexcitability as a result of endothelial dysfunction due to recent evidence showing the ability of the vasculature to communicate with neurons and affect their firing.[17] Changes in cortical neuronal activity in response to whisker stimulation were examined in

Nemo^{Fl} and Nemo^{beKO} mice. Differences were found when using the same stimulation parameters as those used in OIS experiments. Overall, Nemo^{beKO} mice showed more widespread neuronal activity in the barrel cortex (Figure 6(a) and (c)), which was quantified as the peak amplitude of the first peak (Figure 6 (b)), or the average peak amplitude over the entire 20 s stimulation period (Figure 6(c) and (d), left panel). The
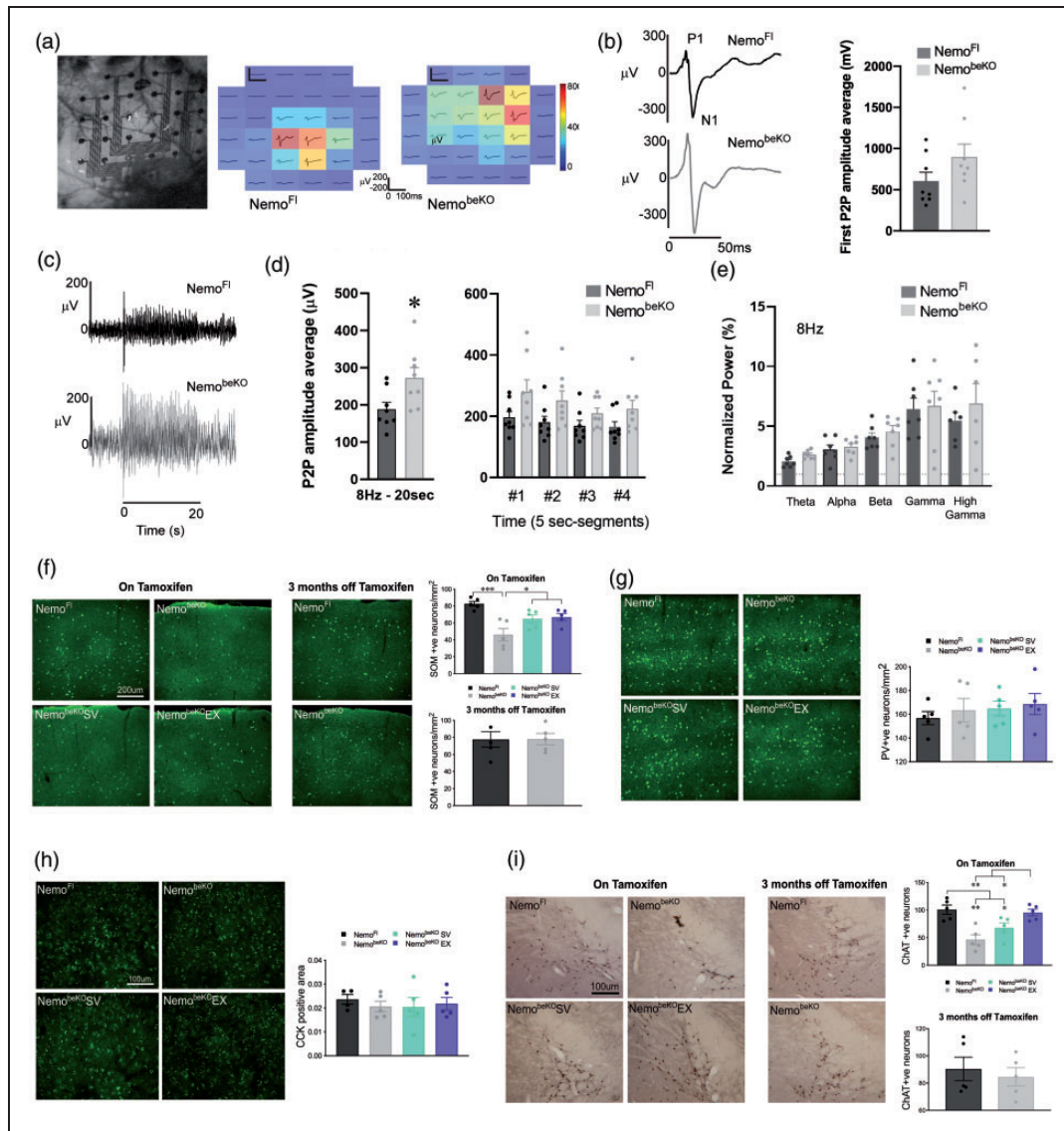

Figure 6. Nemo^{beKO} mice show signs of reduced sensory adaption accompanied by a decreased number of somatostatin (SOM) positive neurons. (A) Representative whisker-evoked neuronal responses (first peaks average, 8 Hz, 20 s stimulation) over the barrel cortex. (B) P1-N1 amplitude example traces and quantifications of first peak showed a trend for Nemo^{beKO} mice to have higher amplitude as compared to Nemo^{Fl} controls with an 8 Hz whisker stimulation frequency. (C) Representative stimulation trains of an 8 Hz stimulation for 20 s. (D) Quantification of peak amplitude average over 20 s stimulation train showed larger responses in Nemo^{beKO} mice ($p < 0.05$), with similar trends at each 5 s segment over the entire stimulation period. (E) When electrophysiological responses were separated into different frequency bands no group differences were observed. $N = 8$/group. Unpaired samples t-tests were used to compare Nemo^{beKO} and Nemo^{Fl} groups for electrophysiology experiments. There was a loss of SOM positive neurons in the barrel cortex of Nemo^{beKO} mice that was not observed in the Nemo^{beKO} mice that exercised (EX) or were treated with simvastatin (SV), and this loss was not seen in the recovery cohort following 3 months off tamoxifen (F). In contrast, no differences in parvalbumin- (PV, G) or cholecystokinin- (CCK, H) containing cortical interneurons in the barrel cortex were observed. There was a significant decrease in the number of choline acetyltransferase (ChAT) positive neurons in the basal forebrain of Nemo^{beKO} mice that was slightly improved by SV and fully protected by EX, and which returned to Nemo^{Fl} levels in the recovery cohort (I). $N = 4$–5 mice/ group and one-way ANOVA with post-hoc Newman-Keuls multiple comparison tests were performed for immunohistochemistry analysis *$p < 0.05$, **$p < 0.01$, ***$p < .001$.

latter reflected changes occurring throughout the stimulation period (Figure 6(d), right panel). When the average peak amplitude was calculated over the entire 20 s period, Nemo[beKO] mice had a higher peak amplitude ($p < 0.05$, Figure 6(d)) of 271 µV ± 28 compared to Nemo[Fl] mice (188 µV ± 19). This difference did not appear to be driven by any particular frequency band (Figure 6(e)).

Amongst other roles, cortical inhibitory neurons have been linked to cognition, which prompted further investigation of the observed altered neuronal activity. Some evidence implicates the loss of interneurons, particularly SOM-expressing interneurons in both VCID[45,46] and AD,[47] as well as loss of PV interneurons in social memory[48] and memory consolidation.[49] When staining for subsets of inhibitory interneurons we found a significant decrease in SOM positive cells in the barrel cortex of Nemo[beKO] mice ($p < 0.001$) that was protected against by both SV and EX treatments ($p < 0.05$) and returned to normal in the recovery cohort (Figure 6(f)). In contrast, there was no difference in the number of PV and CCK interneurons among all groups (Figure 6(g) and (h)). As SOM interneurons are a major target of cholinergic basalocortical afferents,[50] basal forebrain ChAT positive neurons were quantified and found to be reduced in Nemo[beKO] mice compared to Nemo[Fl] mice ($p < 0.01$). This deficit was partially, albeit not significantly recovered by SV, fully normalized by EX, and not detected in the recovery cohort (Figure 6(i)).

Discussion

The main finding from this study is that a healthy endothelium is central to preserving cognitive health as it was not possible for SV, and increasingly difficult for EX to exert their usual beneficial effects on cognition[19,20] in Nemo[beKO] mice with transient dysfunction of brain ECs. This conclusion is further supported by the recovery cohort, in which mice given 3 months to restore EC function displayed reduced pathology and normalized behaviour. Our findings strengthen the hypothesis that damage to the cerebral endothelium is key to initiating pathogenic events that ultimately may lead to dementia.

Links between cerebral ECs and behavioural function

EC disruption has often been associated with cognitive decline,[8,14,51–54] but not extensively studied as a causal factor of brain dysfunction. Here, we show that selective deletion of Nemo in brain ECs was sufficient to cause alterations in cognitive function that are in line with early cognitive symptoms in human patients including olfactory deficits[55] and impaired social interactions.[56] Such changes in Nemo[beKO] mice included impaired olfactory memory, poorer social function, and impoverished nesting behaviour, along with motor deficits. Furthermore, we showed that recovery of EC function fully restored social and nesting behaviours, whereas SV treatment failed to protect against the observed deficits, pointing to ECs as an important target for SV to confer its benefits. EX exerted partial benefits on social behaviour in Nemo[beKO] mice, despite being under the influence of tamoxifen. This may be due to the limited protective effect of EX on endothelium-dependent function depicted here with ACh and the TRPV4 channel opener, hence leading to improved neurovascular interactions essential for cognitive health, as recently shown for cognitive impairments related to high dietary salt.[15]

Consequences of BBB disruptions

When disrupting normal brain EC function of Nemo, we observed BBB leakage featured by increased diffusion of horseradish peroxidase into the parenchyma. This BBB alteration was accompanied by microbleeds, and increased string vessel pathology. Further evidence of a disrupted BBB was the presence of peripheral leukocytes in Nemo[beKO] mice parenchyma. None of these BBB alterations were protected against or reversed by SV or EX despite their known benefits on disrupted EC function,[23,57,58] and ability to tighten the BBB,[59] respectively. Such BBB disruptions likely allowed for a marked increase in neuroinflammation in Nemo[beKO] mice, evidenced by reactive astrocytes, increased microgliosis, and appearance of galectin-3 labeled microglia selectively in WM tracts. Despite EX's often reported potent anti-inflammatory effects,[19,60,61] it failed to quell these neuroinflammatory responses in Nemo[beKO] mice, with the exception of microglial activation. Of interest, BBB breakdown in the hippocampus has been identified as an early biomarker of cognitive dysfunction, and it developed together with brain capillary damage.[13] Furthermore, MRI studies report that patients with preclinical AD have more microbleeds and iron accumulation in their brains compared to healthy elderly controls.[62] Our findings support that subtle disruption in EC function can lead to the extravasation of neurotoxic molecules from the blood, such as thrombin and fibrinogen, causing the brain's glial cells to be in a state of chronic activation, which could lead to neuronal injury.[3,4] It is also possible that the structural damage incurred on the cerebral endothelium triggered a disruption in cerebrovascular reactivity that resulted in a state of hypoperfusion, which was irreversible by SV or EX.

The role of the endothelium in cerebrovascular and neuronal function

Being more than a structural component of the neurovascular unit, the endothelium maintains and regulates the environment to ensure normal neuronal activity, as recently shown in mice fed a high salt diet[15] as blood vessels are responsible for the delivery of essential nutrients and oxygen and the removal of metabolic waste in the brain, compromising EC function can have severe consequences on the brain's homeostasis and impair blood flow dynamics. When we measured artery reactivity, we found that the archetypal endothelial-dependent dilations to ACh and a TRPV4 channel opener were reversed to vasoconstrictions in Nemo[beKO] mice. Such aberrant responses were significantly reduced in mice that exercised compared to untreated mice or mice treated with SV, pointing to healthier ECs following EX.[19,27,63]

The enhanced astrocyte activation in Nemo[beKO] mice could underlie the impaired neurovascular coupling responses to whisker stimulation, possibly by a loss of astrocytic contact along vessel walls[64] or failure to release glial-derived vasoactive mediators.[65] Alternatively, it could point to the important role of ECs in neurovascular co\upling in rapidly propagating stimulus-evoked parenchymal hyperemia to distant pial arteries, as demonstrated using a local, focused or wide light-dye disruption of EC signaling.[66] Our findings in Nemo[beKO] mice expand on this key role for ECs and further show that hemodynamic responses can be fully normalized when EC function is restored. Reduced CBF lowers the rate of nutrient and oxygen delivery, leading to diminished synthesis of ATP required to maintain the sodium-potassium pump involved in action potential firing.[67] Chronic cerebral hypoperfusion may thus lead to an energy deficit severe enough to compromise neurons. This is compatible with the finding that shows altered microvascular tone affects neuronal firing.[17] Although the hypoperfusion experienced by the Nemo[beKO] mice was not chronic, it may have been severe enough to disturb more susceptible neuronal populations and their firing.

In this respect, when investigating cortical inhibitory interneuron populations in Nemo[beKO] mice, we found a selective decrease in SOM-containing interneurons that was not seen in mice treated with SV or EX. Interestingly, decreased SOM levels in specific cortical areas have been found in subjects with dementia,[45,46,68,69] and a similar decrease in SOM neurons was found in the hippocampus in the APP/PS1 model of AD.[47] This decrease in the SOM population also ties in to our electrophysiology findings of increased peak amplitudes during sensory stimulation at 8 Hz, wherein Nemo[beKO] mice displayed impaired sensory adaptation, defined as a reduction in response amplitude to higher sensory stimulus frequencies, and SOM interneurons have been implicated in this phenomenon that limits the processing of extraneous stimuli.[70,71] Furthermore, SOM interneurons are the main target of basalocortical cholinergic afferents,[50] for which originating neurons in the basal forebrain were decreased in Nemo[beKO] mice (Figure 6(i)), possibly affecting their capacity to modulate processing of sensory-evoked cortical activity and hemodynamic responses.[72] SOM and ChAT populations were indistinguishable in the recovery cohort, and the benefits of SV and EX on these neurons did not suffice to reinstate behavior.

Conclusions

In this study, we provide a direct link between a disturbed brain endothelium and late-life dementia by showing that it is possible to induce pathologies observed in VCID and AD by eliciting cerebral EC dysfunction, which was sufficient to trigger mild cognitive deficits. Selective EC deletion of Nemo resulted in BBB disruption, CBF dysregulation, neuroinflammation, together with mild neuronal dysfunction and early trends of disorganized WM tracts, all of which have been implicated in the development and progression of dementia.[4,18] Although the pathological sequence of events following the initial deletion of Nemo in the brain's endothelium is not known, it is likely that the pathologies more closely linked to the endothelium such as BBB breakdown and CBF deficits occur first, which would be proceeded by strong neuroinflammatory responses. Then, due to WM's higher susceptibility than gray matter to reductions in CBF, altered axonal communication may appear next and lead to disruptions in neuronal networks. Of importance, we showed that neither SV nor EX could overcome these pathologies in Nemo[beKO] mice under tamoxifen influence, but that such pathologies were readily normalized when EC function was allowed to recover. This allows us to conclude that SV and EX require a healthy cerebral endothelium to mediate their beneficial effects. Finally, we conclude that a dysfunctional endothelium can be a key initial insult in the development of VCID and maintaining the cerebral endothelium's functional integrity is an important therapeutic strategy to protect against dementia.

Significance statement

We show causative evidence that the transient dysfunction of the cerebral endothelium is an important initial event that leads to early cognitive decline and that subsequent recovery is sufficient to recover cognitive function. We found that neither simvastatin nor exercise

were able to exert their typical neuroprotective benefits when the cerebral endothelium was rendered dysfunctional. Our findings indicate that brain endothelial cells could be a novel and necessary target for effective therapeutic interventions in the prevention of vascular cognitive impairment and dementia.

Declaration of conflicting interests

The author(s) declared no potential conflicts of interest with respect to the research, authorship, and/or publication of this article.

Authors' contributions

Conceptualization, L.J.T., M.S., and E.H; Investigation: L.J.T., M.B., M.L.A., C.L., A.H., and S.S.; Formal Analysis: L.J.T., M.B., M.L.A., C.L., A.H., S.S., and D.J.F.; Visualization: L.J.T., M.B., M.L.A., C.L., S.S.; Software: M.B., C.L. and F.S.; Resources: J.G.S., F.L., M.S., and E.H.; Writing – original draft: L.J.T.; Writing – reviewing and editing: L.J.T., and E.H.; Funding acquisition: M.S. and E.H.; Supervision: E.H.

Supplemental material

Supplemental material for this article is available online.

ORCID iDs

Lianne J Trigiani https://orcid.org/0000-0002-6332-7903
Darren J Fernandes https://orcid.org/0000-0002-0625-7515
Markus Schwaninger https://orcid.org/0000-0002-4510-9718

References

1. Attems J and Jellinger K. The overlap between vascular disease and Alzheimer's disease – lesson from pathology. *BMC Med* 2014; 12: 206–212.
2. de la Torre JC. Alzheimer disease as a vascular disorder. *Stroke* 2002; 33: 1152–1162.
3. Muller K, Courtois G, Ursini MV, et al. New insight into the pathogenesis of cerebral small-vessel diseases. *Stroke* 2017; 48: 520–527.
4. Nelson AR, Sweeney MD, Sagare AP, et al. Neurovascular dysfunction and neurodegeneration in dementia and Alzheimer's disease. *Biochim Biophys Acta* 2016; 1862: 887–900.
5. Grammas P. Neurovascular dysfunction, inflammation and endothelial activation: implications for the pathogenesis of Alzheimer's disease. *J Neuroinflammation* 2011; 8: 26.
6. Lyros E, Bakogiannis C, Liu Y, et al. Molecular links between endothelial dysfunction and neurodegeneration in Alzheimer's disease. *Curr Alzheimer Res* 2014; 11: 18–26.
7. Ridder DA, Wenzel J, Muller K, et al. Brain endothelial TAK1 and NEMO safeguard the neurovascular unit. *J Exp Med* 2015; 212: 1529–1549.
8. Sweeney MD, Kisler K, Montagne A, et al. The role of brain vasculature in neurodegenerative disorders. *Nat Neurosci* 2018; 21: 1318–1331.
9. Villaseñor R, Lampe J, Schwaninger M, et al. Intracellular transport and regulation of transcytosis across the blood–brain barrier. *Cell Mol Life Sci* 2019; 76: 1081–1092.
10. Sweeney MD, Sagare AP and Zlokovic BV. Blood-brain barrier breakdown in Alzheimer disease and other neurodegenerative disorders. *Nat Rev Neurol* 2018; 14: 133–150.
11. Zlokovic B. Neurovascular pathways to neurodegeneration in Alzheimer's disease and other disorders. *Nat Rev Neurosci* 2011; 12: 723–738.
12. Iturria-Medina Y, Sotero RC, Toussaint PJ, et al.; Alzheimer's Disease Neuroimaging Initiative. Alzheimer's disease neuroimaging I. Early role of vascular dysregulation on late-onset Alzheimer's disease based on multifactorial data-driven analysis. *Nat Commun* 2016; 7: 11934.
13. Nation DA, Sweeney MD, Montagne A, et al. Blood-brain barrier breakdown is an early biomarker of human cognitive dysfunction. *Nat Med* 2019; 25: 270–276.
14. Toth P, Tarantini S, Csiszar A, et al. Functional vascular contributions to cognitive impairment and dementia: mechanisms and consequences of cerebral autoregulatory dysfunction, endothelial impairment, and neurovascular uncoupling in aging. *Am J Physiol Heart Circ Physiol* 2017; 312: H1–H20.
15. Faraco G, Hochrainer K, Segarra SG, et al. Dietary salt promotes cognitive impairment through tau phosphorylation. *Nature* 2019; 574: 686–690.
16. Di Marco LY, Venneri A, Farkas E, et al. Vascular dysfunction in the pathogenesis of Alzheimer's disease – a review of endothelium-mediated mechanisms and ensuing vicious circles. *Neurobiol Dis* 2015; 82: 593–606.
17. Kim KJ, Ramiro Diaz J, Iddings JA, et al. Vasculo-neuronal coupling: retrograde vascular communication to brain neurons. *J Neurosci* 2016; 36: 12624–12639.
18. Wang F, Cao Y, Ma L, et al. Dysfunction of cerebrovascular endothelial cells: prelude to vascular dementia. *Front Aging Neurosci* 2018; 10: 376.

19. Trigiani LJ, Royea J, Tong X-K, et al. Comparative benefits of simvastatin and exercise in a mouse model of vascular cognitive impairment and dementia. *Faseb J* 2019; 33: 13280–13293.

20. Tong XK, Trigiani LJ and Hamel E. High cholesterol triggers white matter alterations and cognitive deficits in a mouse model of cerebrovascular disease: benefits of simvastatin. *Cell Death Dis* 2019; 10: 89.

21. McGirt MJ, Lynch JR, Parra A, et al. Simvastatin increases endothelial nitric oxide synthase and ameliorates cerebral vasospasm resulting from subarachnoid hemorrhage. *Stroke* 2002; 33: 2950–2956.

22. Carneado J, Sotomayor MAd, Perez-Guerrero C, et al. Simvastatin improves endothelial function in spontaneously hypertensive rats through a superoxide dismutase mediated antioxidant effect. *J Hypertens* 2002; 20: 429–437.

23. van Nieuw Amerongen G, Vermeer M, Nègre-Aminou P, et al. Simvastatin improves disturbed endothelial barrier function. *Circulation* 2000; 102: 2803–2809.

24. Barnes JN and Corkery AT. Exercise improves vascular function, but does this translate to the brain? *Brain Plast* 2018; 4: 65–79.

25. Choi JK, Moon KM, Jung SY, et al. Regular exercise training increases the number of endothelial progenitor cells and decreases homocysteine levels in healthy peripheral blood. *Korean J Physiol Pharmacol* 2014; 18: 163–168.

26. Defina LF, Willis BL, Radford NB, et al. The association between midlife cardiorespiratory fitness levels and later-life dementia: a cohort study. *Ann Intern Med* 2013; 158: 162–168.

27. Trigiani LJ and Hamel E. An endothelial link between the benefits of physical exercise in dementia. *J Cereb Blood Flow Metab* 2017; 37: 2649–2664.

28. Percie Du Sert N, Hurst V, Ahluwalia A, et al. The ARRIVE guidelines 2.0: updated guidelines for reporting animal research. *PLoS Biol* 2020; 18: e3000410.

29. Deipolyi AR, Fang S, Palop JJ, et al. Altered navigational strategy use and visuospatial deficits in hAPP transgenic mice. *Neurobiol Aging* 2008; 29: 253–266.

30. Royea J, Zhang L, Tong XK, et al. Angiotensin IV receptors mediate the cognitive and cerebrovascular benefits of losartan in a mouse model of Alzheimer's disease. *J Neurosci* 2017; 37: 5562–5573.

31. Deacon RM. Assessing nest building in mice. *Nat Protoc* 2006; 1: 1117–1119.

32. Tong XK, Nicolakakis N, Kocharyan A, et al. Vascular remodeling versus amyloid beta-induced oxidative stress in the cerebrovascular dysfunctions associated with Alzheimer's disease. *J Neurosci* 2005; 25: 11165–11174.

33. Dubeau S, Desjardins M, Pouliot P, et al. Biophysical model estimation of neurovascular parameters in a rat model of healthy aging. *Neuroimage* 2011; 57: 1480–1491.

34. Bock NA, Nieman BJ, Bishop JB, et al. In vivo multiple-mouse MRI at 7 tesla. *Magn Reson Med* 2005; 54: 1311–1316.

35. Jones D, Horsfield M and Simmons A. Optimal strategies for measuring diffusion in anisotropic systems by magnetic resonance imaging. *Magn Reson Med* 1999; 42: 515–525.

36. Friedel M, van Eede MC, Pipitone J, et al. Pydpiper: a flexible toolkit for constructing novel registration pipelines. *Front Neuroinform* 2014; 8: 67–21.

37. Collins D, Neelin P, Peters T, et al. Automatic 3D inter-subject registration of MR volumetric data in standardized Talairach space. *J Comput Assist Tomogr* 1994; 18: 192–205.

38. Avants BB, Tustison NJ, Song G, et al. A reproducible evaluation of ANTs similarity metric performance in brain image registration. *Neuroimage* 2011; 54: 2033–2044.

39. Steadman PE, Ellegood J, Szulc KU, et al. Genetic effects on cerebellar structure across mouse models of autism using a magnetic resonance imaging atlas. *Autism Res* 2014; 7: 124–137.

40. Qiu LR, Fernandes DJ, Szulc-Lerch KU, et al. Mouse MRI shows brain areas relatively larger in males emerge before those larger in females. *Nat Commun* 2018; 9: 2615.

41. Genovese CR, Lazar NA and Nichols T. Thresholding of statistical maps in functional neuroimaging using the false discovery rate. *Neuroimage* 2002; 15: 870–878.

42. Morino P, Herrera-Marschitz M, Castel MN, et al. Cholecystokinin in cortico-striatal neurons in the rat: immunohistochemical studies at the light and electron microscopical level. *Eur J Neurosci* 1994; 6: 681–692.

43. Benitez A, Fieremans E, Jensen JH, et al. White matter tract integrity metrics reflect the vulnerability of late-myelinating tracts in Alzheimer's disease. *Neuroimage Clin* 2014; 4: 64–71.

44. Deacon RM. Measuring the strength of mice. *J Vis Exp* 2013; 75: e2609.

45. Holm H, Nägga K, Nilsson ED, et al. N-Terminal pro-somatostatin and risk of vascular dementia. *Cerebrovasc Dis* 2017; 44: 259–265.

46. Shen Y and Gao H-M. Serum somatostatin and neuron-specific enolase might be biochemical markers of vascular dementia in the early stage. *Int J Clin Exp Med* 2015; 8: 19471–19475.

47. Schmid LC, Mittag M, Poll S, et al. Dysfunction of somatostatin-positive interneurons associated with memory deficits in an Alzheimer's disease model. *Neuron* 2016; 92: 114–125.

48. Deng X, Gu L, Sui N, et al. Parvalbumin interneuron in the ventral hippocampus functions as a discriminator in social memory. *Proc Natl Acad Sci USA* 2019; 116: 16583–16592.

49. Xia F, Richards BA, Tran MM, et al. Parvalbumin-positive interneurons mediate neocortical-hippocampal interactions that are necessary for memory consolidation. *Elife* 2017; 6: e27868.

50. Cauli B, Tong XK, Rancillac A, et al. Cortical GABA interneurons in neurovascular coupling: relays for subcortical vasoactive pathways. *J Neurosci* 2004; 24: 8940–8949.

51. Madigan JB, Wilcock DM and Hainsworth AH. Vascular contributions to cognitive impairment and

dementia: topical review of animal models. *Stroke* 2016; 47: 1953–1959.

52. Brown WR, Moody DM, Thore CR, et al. Microvascular changes in the white mater in dementia. *J Neurol Sci* 2009; 283: 28–31.

53. Uiterwijk R, Huijts M, Staals J, et al. Endothelial activation is associated with cognitive performance in patients with hypertension. *Am J Hypertens* 2016; 29: 464–469.

54. Adamski MG, Sternak M, Mohaissen T, et al. Vascular cognitive impairment linked to brain endothelium inflammation in early stages of heart failure in mice. *J Am Heart Assoc* 2018; 7: e007694.

55. Devanand D, Lee S, Manly J, et al. Olfactory deficits predict cognitive decline and Alzheimer dementia in an urban community. *Neurology* 2015; 84: 182–189.

56. Nyenhuis D and Gorelick P. Diagnosis and management of vascular cognitive impairment. *Curr Atheroscler Rep* 2007; 9: 326–332.

57. Jiang X, Guo M, Su J, et al. Simvastatin blocks blood-brain barrier disruptions induced by elevated cholesterol both in vivo and in vitro. *Int J Alzheimers Dis* 2012; 2012: 109324.

58. Yang D, Knight RA, Han Y, et al. Statins protect the blood brain barrier acutely after experimental intracerebral hemorrhage. *Jbbs* 2013; 03: 100–106.

59. Souza PS, Gonçalves ED, Pedroso GS, et al. Physical exercise attenuates experimental autoimmune encephalomyelitis by inhibiting peripheral immune response and blood-brain barrier disruption. *Mol Neurobiol* 2017; 54: 4723–4737.

60. Małkiewicz MA, Szarmach A, Sabisz A, et al. Blood-brain barrier permeability and physical exercise. *J Neuroinflammation* 2019; 16: 15.

61. Mee-Inta O, Zhao ZW and Kuo YM. Physical exercise inhibits inflammation and microglial activation. *Cells* 2019; 8: 691.

62. Yates PA, Desmond PM, Phal PM, et al.; For the AIBL Research Group. Incidence of cerebral microbleeds in preclinical Alzheimer disease. *Neurology* 2014; 82: 1266–1273.

63. Bolduc V, Thorin-Trescases N and Thorin E. Endothelium-dependent control of cerebrovascular functions through age: exercise for healthy cerebrovascular aging. *Am J Physiol Heart Circ Physiol* 2013; 305: H620–H633.

64. Duncombe J, Lennen RJ, Jansen MA, et al. Ageing causes prominent neurovascular dysfunction associated with loss of astrocytic contacts and gliosis. *Neuropathol Appl Neurobiol* 2017; 43: 477–491.

65. Filosa JA, Morrison HW, Iddings JA, et al. Beyond neurovascular coupling, role of astrocytes in the regulation of vascular tone. *Neuroscience* 2016; 323: 96–109.

66. Chen BR, Kozberg MG, Bouchard MB, et al. Critical role for the vascular endothelium in functional neurovascular coupling in the brain. *J Am Heart Assoc* 2014; 3: e000787.

67. Harris JJ, Jolivet R and Attwell D. Synaptic energy use and supply. *Neuron* 2012; 75: 762–777.

68. Dournaud P, Delaere P, Hauw JJ, et al. Differential correlation between neurochemical deficits, neuropathology, and cognitive status in Alzheimer's disease. *Neurobiol Aging* 1995; 16: 817–823.

69. Epelbaum J, Javoy-Agid F, Enjalbert A, et al. Somatostatin concentrations and binding sites in human frontal cortex are differentially affected in Parkinson's disease associated dementia and in progressive supranuclear palsy. *J Neurol Sci* 1988; 87: 167–174.

70. Latimer KW, Barbera D, Sokoletsky M, et al. Multiple timescales account for adaptive responses across sensory cortices. *J Neurosci* 2019; 39: 10019–10033.

71. Riedemann T. Diversity and function of somatostatin-expressing interneurons in the cerebral cortex. *Int J Mol Sci* 2019; 20: 2952.

72. Lecrux C, Sandoe CH, Neupane S, et al. Impact of altered cholinergic tones on the neurovascular coupling response to whisker stimulation. *J Neurosci* 2017; 37: 1518–1531.